spherical wave. It enables faster calculations with much higher accuracy.

This becomes absolutely necessary when one is interested in the study of the direct image. As will be explained in another paper, it permits the real width of the X-ray beam incident on the crystal to be taken into account and one may now obtain simulations of very high quality.

We can already announce that the VSA is accurate enough to allow the simulation of traverse topographs. The work is in progress and the first results are very satisfactory.

Most of the tests were done at the IBM J. J. Watson Research Center in Yorktown Heights during time spent as a 'World Trade Scientist Visitor'.

I would like to thank A. Soyer for the final debugging of the corresponding simulation program.

References

AUTHIER, A. (1967). *Adv. X-ray. Anal.* **10**, 9–31.
AUTHIER, A., MALGRANGE, C. & TOURNARIE, M. (1968). *Acta Cryst.* A**24**, 126–136.
BALIBAR, F. & AUTHIER, A. (1967). *Phys. Status Solidi*, **21**, 413–422.
BEDYNSKA, T., BUBAKOVA, R. & SOUREK, Z. (1976). *Phys. Status Solidi A*, **36**, 509–515.
CHUKOVSKII, T. N. (1974). Proc. 2nd ECM, Kesthely, Hungary.
EPELBOIN, Y. (1974). *J. Appl. Cryst.* **7**, 372–377.
EPELBOIN, Y. (1975). *Acta Cryst.* A**31**, 591–599.
EPELBOIN, Y. (1977). *Acta Cryst.* A**33**, 758–767.
EPELBOIN, Y. (1979). *J. Appl. Phys.* **50**, 1312–1317.
ISHIDA, H., MIYAMOTO, N. & KOHRA, K. (1976). *J. Appl. Cryst.* **9**, 240–241.
KATO, N. (1961). *Acta Cryst.* **14**, 627–635.
MILTAT, J. & BOWEN, D. K. (1975). *J. Appl. Cryst.* **8**, 657–669.
NOURTIER, C., KLEMAN, M., TAUPIN, D., MILTAT, J., LABRUNE, M. & EPELBOIN, Y. (1979). *J. Appl. Phys.* **50**, 2143–2145.
NOURTIER, C. & TAUPIN, D. (1983). In preparation.
PETRASHEN, P. V. (1976). *Fiz. Tverd. Tela (Leningrad)*, **18**, 3729–3731.
RIGLET, P., SAUVAGE, M., PETROFF, J. F. & EPELBOIN, Y. (1980). *Philos. Mag.* A**3**, 339–358.

Acta Cryst. (1983). A**39**, 767–772

Theoretical Study of the Influence of the Width of the Entrance Slit on the Contrast of Dislocations in X-ray Topography by Means of Simulations

BY Y. EPELBOIN AND A. AUTHIER

Laboratoire de Minéralogie–Cristallographie, associé au CNRS, Université P. et M. Curie and Paris VII, 75230 Paris CEDEX 05, France

(*Received* 18 *January* 1983; *accepted* 10 *May* 1983)

Abstract

Experimental topographs may be simulated by addition of simulations where one point source is lit on the surface of the crystal. The accuracy of a varying-step integration of Takagi equations is good enough to allow such computations. It is shown that all parts of the contrast are sensitive to the width of the entrance slit and that accurate characterization of defects must take this parameter into account.

Introduction

X-ray topography (Lang, 1959) is a very useful tool for studying the perfection of crystalline materials. The most widely used method, translation topography, allows the characterization of a large volume of the crystal in a single experiment.

Section topography allows a much more precise study of the defects but the experiment is rather delicate and only a small volume of the material is characterized in one experiment. The quality of the experimental setting, especially the width and parallelism of the entrance slit of the camera, become very important and these parameters should be taken into account in all theoretical and experimental studies. Usually the width of the entrance slit, limiting the incoming beam falling on the crystal, is of the order of 10 μm in section topographs and may be increased to values of the order of 100 μm or more in traverse topography.

It is well known that the quality and number of extinction fringes visible in a section topograph depend not only on the perfection of the crystal but also on the accuracy of the setting and on the width of the incoming beam. The narrower the slit is, the greater will be the number of observable fringes. Of course this is limited by the intensity of the X-ray beam!

0108-7673/83/050767-06$01.50

In theoretical studies of the contrast the use of simulations is now a very important method for understanding the image and fully characterizing the defects. For instance, it is possible to determine the direction and magnitude of the Burgers vector of a dislocation (Epelboin, 1974) and to characterize ferromagnetic walls (Nourtier, Kleman, Taupin, Miltat, Labrune & Epelboin, 1979) or planar defects (Capelle, Epelboin & Malgrange, 1982).

As will be explained later, simulations are computed, in most cases, by simulating one point source on the entrance surface of the crystal; the accuracy of the numerical integration does not allow the real experimental width of the incoming beam to be taken into account. Recently, new algorithms using a varying integration step have been developed (Petrashen, 1976; Epelboin, 1981) and their accuracy allows this experimental factor to be taken into account.

First, we will discuss the approximation of the incident spherical wave and its extension to real experiments. Then we will briefly recall the basic principles of simulations using a varying integration step. In the third part we will show through some examples of silicon and quartz how the width of the entrance slit modifies the contrast of a dislocation and how, taking this point into account, it is possible to simulate section topographs with very high accuracy.

I. Theoretical considerations

1. *Classification of the various topographic settings*

From the theoretical point of view we may consider three kinds of topographic settings:

(*a*) The source is a point source situated on the entrance surface of the crystal and may be expressed as a Dirac distribution.

(*b*) The source is a plane wave and thus its lateral extension is infinite.

(*c*) Traverse topography, which may be obtained either by scanning the point source along the surface of the crystal or by giving all possible orientations to a plane wave along the rocking curve of the reflection.

In the first two cases the amplitude distributions are Fourier transforms, thus the integrated intensity (*c*) is identical in both cases. In real experiments (*a*) and (*b*) do not exist and may be obtained approximately by using either a narrow slit (*a*) (Fig. 1) or a special setting in order to obtain a wave with a large lateral extension and a very limited angular distribution (multiple-crystal topography, synchrotron topography).

2. *The approximation of the point source* (*Kato*, 1961)

Let Ω_0 be the angle in which the angular spectrum of the coherent incident wave takes an appreciable value.

The incident wave may be approximated as a plane wave if $\delta \gg \Omega$, where δ is the width at half maximum of the rocking curve. Ω_o may be approximated as the geometrical width of the incident beam. Using an entrance slit 10 μm wide means that $\Omega_0 \simeq 2{\cdot}5 \times 10^{-4}$ rad and δ is of the order of 10^{-5} rad.

Thus the approximation of the plane wave can never be justified for section topography.

A second condition is that $f \gg s$, where f is the width where the phase of the incident wave may be considered as constant along the entrance surface and s the effective crystal size, *i.e.* the length along the surface where the crystal can accommodate the divergence of the incident beam. $s \simeq L\delta$, where L is of the order of 0·4 m, the distance from the focal point to the crystal in most cameras. f is of the order of the width of the first Fresnel zone, *i.e.* $f \simeq 2\ (\lambda\ L)^{1/2}$. This leads to the following relation:

$$2(\lambda/L)^{1/2} \gg \delta,$$

in order to approximate the incident wave as a plane wave. This is very seldom true. Thus we may always assume that the incident wave is a spherical wave of limited lateral extension.

Very recently Aristov, Kohn, Polovinkina & Snigirev (1982) studied the validity of Kato's approximation. Taking into account both the spectral width of the incident beam and the finite width of the incoming beam they have shown that for the usual topographic setting the non-monochromaticity and the dimensions of the focus are the reasons why Kato's theory is valid. Each point of the entrance surface of the crystal acts as an elementary source of spherical waves and the intensity distribution along the exit surface is the summation of all intensities coming from all these sources acting incoherently. The distance L between the focus and the crystal appears only as a constant factor which may be taken into account in the normalization of the intensities. L remains an important factor in the geometrical resolution of the experiment only.

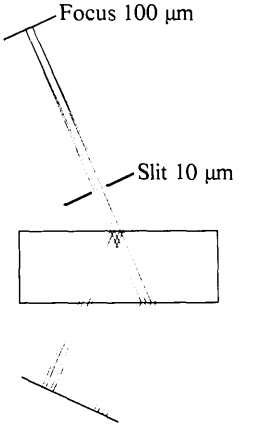

Fig. 1. Principle of section topograph using a limited incident beam.

3. *Boundary conditions along the entrance surface*

Let us recall the well-known Takagi–Taupin equations (Takagi, 1962; Taupin, 1964):

$$\frac{\partial}{\partial s_0} D_0(\mathbf{r}) = -i\pi k\, \chi_h D_h(\mathbf{r})$$

$$\frac{\partial}{\partial s_h} D_h(\mathbf{r}) = -i\pi k\, \chi_h D_0(\mathbf{r}) - 2i\,\pi k \frac{\partial}{\partial s_h} \mathbf{g}.\mathbf{u}(\mathbf{r}) D_h(\mathbf{r}),$$

where χ_h and $\chi_{\bar{h}}$ are the Fourier components of the dielectric susceptibility, $\mathbf{g}$ is the reciprocal-lattice vector corresponding to the reflection and $\mathbf{u}(\mathbf{r})$ is the local deformation inside the crystal.

The boundary conditions along the surface ξ may be written as:

$$D_0(\xi) = D_a(\xi)$$
$$D_h(\xi) = 0$$

$$\frac{\partial D_0}{\partial s_0}(\xi) = 0$$

$$\frac{\partial D_h}{\partial s_h}(\xi) = -i\pi k\, \chi_h D_a(\xi),$$

where $D_a(\xi)$ is the amplitude distribution of the incident wave along the surface.

II. Numerical integration of Takagi–Taupin equations

1. *Integration algorithm*

In the numerical integration the partial-derivative equations are replaced by a step-by-step integration.

Using the half-step derivative method (Authier, Malgrange & Tournarie, 1968) the integration is performed along a network of characteristics parallel to the transmitted and reflected directions $\mathbf{s}_0$ and $\mathbf{s}_h$. The values of the amplitudes D_0 and D_h of the waves at a given point A depend upon the values at points B and C in the integration network (Fig. 2).

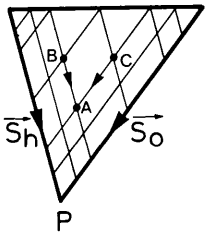

Fig. 2. Principle of the numerical integration.

The first program written to integrate Takagi–Taupin equations used constant steps p and q along both characteristics (Authier *et al.*, 1968). This means that the distances AB and AC are fixed before the computation according to some rules which have been discussed in another paper (Epelboin, 1977):

– The steps p and q must be small enough to take into account the oscillations of the wave fields, especially near the edges of the Borrmann fan.

– p and q must be large enough to avoid numerical errors due to the half-step derivative method and to the limited precision of the computer. Moreover, since the computation time is proportional to $1/p^2$ and $1/q^2$ it is necessary to choose the steps as big as possible.

In practice, it is not possible to take into account the rapid changes of the wavefields near the edges of the Borrmann fan and the intensity due to wavefield interaction in these areas is strongly underestimated. This is not important when one is only interested in the general features of the image but becomes intolerable when one takes into account the finite size of the entrance slit.

Petrashen (1976) and Epelboin (1981) have suggested using an integration network where the steps p and q vary. The difficulty is to find a method which allows these steps to change inside the Borrmann fan. Petrashen suggests decreasing them near the edges of the fan. Epelboin uses a more sophisticated method based on the following idea.

The ideal solution would be to use a finite element method: at each point of the calculation p and q would be chosen according to the local variations of the wave amplitudes. Unfortunately this would need tremendous computation time, which means that the network must be known before starting the integration.

The network is thus chosen for an asymptotic solution, *i.e.* the perfect crystal; we compute the position of the following zeros of the J_0 Bessel function (amplitude of the D_h wave) along the exit surface. Then the position of the nodes is chosen so that a minimum number of points is used to describe the oscillation of this function between two zeros. From these points we draw characteristic lines as shown in Fig. 3. The density of nodes is greater near the edges where the wave amplitudes vary rapidly and decrease in the middle of the fan where they change slowly. In the areas where the dislocation interacts with the refracted beam the density of nodes may be increased. A complete comparison of the varying step algorithm (VSA) *versus* the constant step algorithm (CSA) is given by Epelboin (1983).

2. *Boundary conditions*

According to Aristov *et al.* (1982) boundary conditions along the entrance surface may be simulated by the addition of elementary section topographs,

each corresponding to one point source sited along the surface. This corresponds to Kato's theory.

The number of elementary section topographs needed to simulate the finite width of the incoming beam is determined by the resolution of the calculation. If Δ is the distance between two successive calculated points along the exit surface this must be the distance between the different simulations (Fig. 4*a*).

However, one difficulty appears: the distance between two computed points is not constant. To avoid this problem the array of computed intensities is increased: by interpolation intermediate points are calculated so that the distance between two successive points becomes Δ_{min}, this being the minimum horizontal distance between two nodes in the integration network (Fig. 3). In a second step the number of points is decreased by an apodisation scheme so that the resolution becomes Δ along the exit surface: a given number of points is added two by two. This is repeated many times so as to replace all the points by only one. Then a new packet of points is added in the same manner. Two successive computed intensities are not completely independent: two successive packets possess half of their information in common. This permits a better simulation of the photographic process where neighbouring grains influence each other. This may be explained in a drawing (Fig. 5), each horizontal line in the triangles representing one level of addition. In this example the information is reduced by a factor of three. Thus the distance between two points becomes $\Delta = 3 \times \Delta_{min}$. For example, in most simulations $\Delta_{min} = 0{\cdot}2$ μm. Using an apodisation factor of four means that the resolution will be $0{\cdot}8$ μm. This will also be the distance between two successive sources along the entrance surface. The number of added elementary simulations depends upon the width of the entrance slit and the requested resolution.

This must not be confused with the simulation of a plane-wave topograph where in the same calculation a great number of sources emit coherently along the entrance surface (Fig. 4*b*).

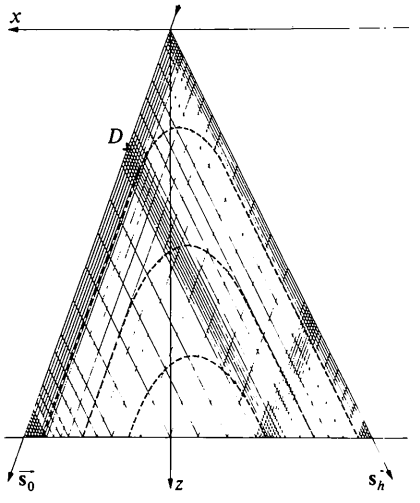

Fig. 3. Integration network for VSA algorithm. The density of knots may be increased in the areas from which the direct image originates.

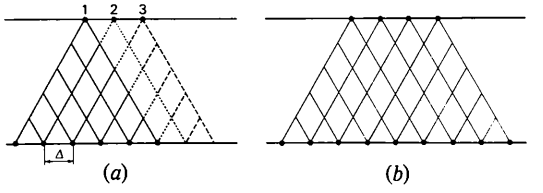

Fig. 4. (*a*) Principle of the simulation of extended section topographs. Single simulations are added. (*b*) Principle of the simulation of a plane-wave topograph. One simulation using an extended wave along the entrance surface.

III. Study of the influence of the entrance slit

1. *The different parts of an image*

Authier (1967) distinguishes three parts in the image of a defect (Fig. 6): the direct image which appears whenever the defect intercepts the refracted beam, the dynamical image which is the shadow of the defect and the intermediary image, rather complex, which corresponds to the interference pattern of all wave fields of which the paths have been disturbed or diffracted by the deformation of the crystal.

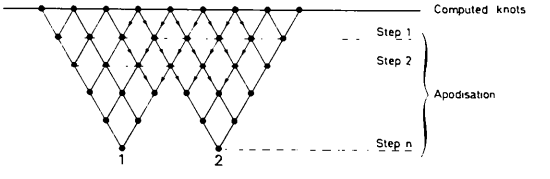

Fig. 5. Summation of the calculated intensities along the exit surface. A given number of points is added two by two and the process is repeated for n steps to reduce the information to one point. This is repeated for a new packet of points, taking half of the information in common.

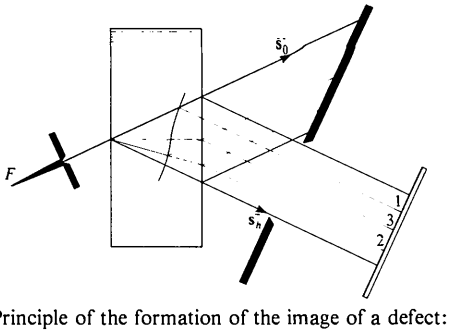

Fig. 6. Principle of the formation of the image of a defect: 1 direct image; 2 dynamical image; 3 intermediary image.

When a dislocation lies parallel to the surface the intermediary image is not clearly visible; when it is inclined this image appears as a set of fringes roughly perpendicular to the dynamical image. This is clearly visible in the topographs shown in Figs. 7(*a*) and 8(*a*).

Fig. 7(*a*) is the image of an inclined dislocation in a silicon wafer. It has been described by Authier (1967). Fig. 8(*a*) is the topograph of dislocation in quartz (Epelboin & Patel, 1982). The corresponding simulations have been computed for various widths of the entrance slit: Figs. 7(*b*) and 8(*b*) lighting with one point source only as is usually done in simulations, Figs. 7(*c*) and 8(*c*) simulating an incoming beam 3 μm wide, Figs. 7(*d*) and 8(*d*) with a slit 9 μm wide.

2. *Study of the background*

It is well known that the number of visible extinction fringes is unrealistic in simulations. When taking into account the finite width of the entrance slit, their number may be reduced as shown in the simulations. An elementary simulation corresponds to Kato's theory and the number of computed fringes is in agreement with it; but in a real experiment their contrast is blurred, due to the addition of all the intensities corresponding to all the incoherent sources along the entrance surface. Since the width of the fringes decreases near the edges of the section topograph, fringes remain visible in the centre of the image only.

This is a good way to check the real width of the entrance slit of a camera and we have been able to do this by comparison of a set of simulations with real experiments: Fig. 8(*d*) shows that the topograph has been taken with an incident beam with a width of about 10 μm. This is not so clearly visible in Fig. 7 but a certain degree of imperfection in the crystal (additional stresses, microdefects, *etc.*) might be the reason.

3. *Study of the direct image*

In Fig. 7 the direct image is rather small because the crystal is deformed in a small volume only around the core of the dislocation. This is not true in Fig. 8 and has been studied in a previous paper (Epelboin & Patel, 1982).

The set of simulations show that the size of this image is sensitive to the width of the beam. Fig. 8(*d*) demonstrates that a detailed study of this part of the contrast cannot be done without taking this factor into account.

In some cases it might become possible to determine the direction and magnitude of the Burgers vector of a dislocation by its study only.

4. *Study of the dynamical image*

Strictly speaking, any part of the contrast results from the convolution of the image given by one point

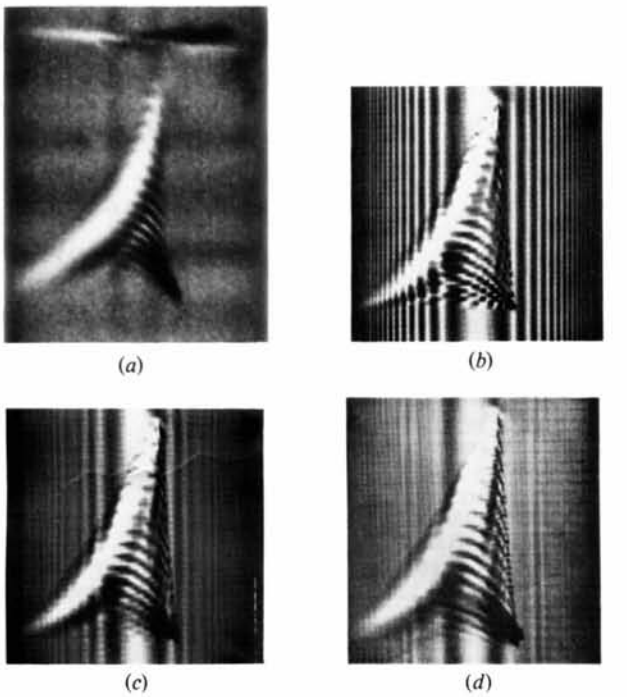

Fig. 7. Section topograph of a dislocation; Si, Mo $K\alpha$, 220, 800 μm thick: (*a*) experiment; (*b*) one point source; (*c*) slit 9 μm (addition of 5 single simulations); (*d*) slit 17·6 μm (addition of 11 single simulations).

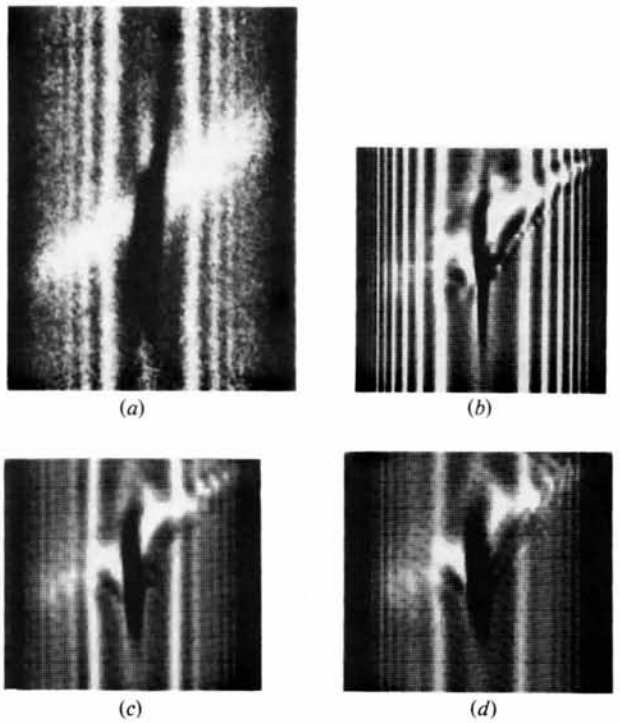

Fig. 8. Section topograph of a dislocation; quartz Ag $K\alpha$, 01T2 (see Epelboin & Patel, 1982): (*a*) experiment; (*b*) one point source; (*c*) slit 6 μm (addition of 5 single simulations); (*d*) slit 10 μm (addition of 5 single simulations).

source with the distribution along the entrance surface. In the case of the dynamical image it is not as easy as for the direct image to predict whether it will be increased or decreased. Figs. 7(*c*) and (*d*) show, for instance, that the image may be slightly larger when the width of the entrance slit increases; on the contrary, Fig. 8 shows the opposite. This is due to the balance between black and white when summing all single topographs and no prediction may be made. The computed image is smaller than the real one. An explanation could be that additional stresses exist such as a slight decoration of the dislocation which would increase the size of the deformed areas in the crystal and thus the size of dynamical image. Since no intermediary image exists it is difficult to draw a conclusion.

5. *Study of the intermediary image*

The intermediary image contains a large portion of the information; its system of fringes is very sensitive to the distribution of the stresses in the Borrmann fan and its study permits a very accurate evaluation of the parameters of the defect. Unfortunately, it is not easy to interpret!

Fig. 7 is a good example. The simulation shown in Fig. 7(*b*) is not very satisfactory for this part of the contrast: flat fringes appear at the bottom of the image and the intensity of those parallel to the dynamical image is not strong enough.

In the series of simulations these effects vanish: the flat fringes are blurred and the contrast of the fringes parallel to the dynamical image is reinforced. The simulation in Fig. 7(*c*) corresponds to an entrance slit 9 μm wide. The difference between the simulation and the experiment suggests the use of an entrance slit larger than expected as shown in Fig. 7(*d*) where the size of the entrance slit is 17·6 μm, which is slightly more in agreement with the experiment.

Moreover, we simulate a perfect dislocation in a perfect crystal for a theoretical setting. This of course never happens in real experiments and may explain some discrepancies.

Conclusion

These examples show that the real width of the entrance slit has to be taken into account for precise simulations of section topographs. As is already known from experiment the features of the image are very sensitive to this factor. The use of a one-point source, although satisfactory for an ordinary characterization of a defect, becomes insufficient when one is interested in a detailed study of the contrast. It also shows the limitation of Kato's theory, in the study of real contrasts.

On the other hand, two difficulties appear:

(*a*) the integration of Takagi–Taupin equations must be done using a varying-step algorithm, otherwise the inaccuracy of the calculation would give false results;

(*b*) the computation time is increased since many single simulations must be added.

This limiting factor is not crucial. The varying-step algorithm is faster than the old constant-step algorithm. The utilization of modern computers speeds up the calculation. An image such as the one shown in Fig. 7(*c*) which corresponds to the addition of five single simulations may be computed in less than 40 min, using a microcomputer MINI6/53 CII-HB (comparable in speed to a DEC 11-70) linked to a FPS 100 array processor. The final image is thus obtained in a shorter time than that needed for a single simulation using an IBM 370/168.

In the future, detailed studies of real topographs using such simulations may permit one to overcome the physical limitation due to the geometrical resolution of photographic emulsions and allow a better characterization of large volumes of crystalline materials.

Part of this work was done at the IBM T. J. Watson Research Center (Yorktown Heights, USA). One of us (YE) is greatly indebted to IBM World Trade and IBM France for a grant.

We thank F. Morris and A. Soyer for help in the use of the array processor.

References

ARISTOV, V. V., KOHN, V. G., POLOVINKINA, V. I. & SNIGIREV, A. A. (1982). *Phys. Status Solidi A*, **72**, 483–491.

AUTHIER, A. (1967). *Adv. X-ray Anal.* **10**, 9–31.

AUTHIER, A., MALGRANGE, C. & TOURNARIE, M. (1968). *Acta Cryst.* A**24**, 126–136.

CAPELLE, B., EPELBOIN, Y. & MALGRANGE, C. (1982). *J. Appl. Phys.* **53**, 10, 6767–6771.

EPELBOIN, Y. (1974). *J. Appl. Cryst.* **7**, 372–377.

EPELBOIN, Y. (1977). *Acta Cryst.* A**31**, 591–599.

EPELBOIN, Y. (1981). *Acta Cryst.* A**37**, 132–133.

EPELBOIN, Y. (1983). *Acta Cryst.* A**39**, 761–767.

EPELBOIN, Y. & PATEL, J. R. (1982). *J. Appl. Phys.* **53**, 271–275.

KATO, N. (1961). *Acta Cryst.* **14**, 627–635.

LANG, A. R. (1959). *J. Appl. Phys.* **30**, 1748–1755.

NOURTIER, C., KLEMAN, M., TAUPIN, D., MILTAT, J., LABRUNE, M. & EPELBOIN, Y. (1979). *J. Appl. Phys.* **50**, 3, 2143–2145.

PETRASHEN, P. V. (1976). *Fiz. Tverd. Tela* (*Leningrad*), **18**, 3729–3731.

TAKAGI, S. (1962). *Acta Cryst.* **23**, 23–25.

TAUPIN, D. (1964). *Bull. Soc. Fr. Minéral. Cristallogr.* **87**, 469–511.